slightly soluble in iron metal at the pressure of the CMB (*23*), Reaction 1 represents a net transfer of FeO to ferropericlase. The residual Fe-FeS liquid is probably immiscible with the lower mantle and either drains back to the core or crystallizes within the lower mantle as Fe-FeS veins. Thus, large regions of the lower mantle may be metasomatized by FeO-bearing liquids creating high Fe/Mn sources, with siderophile Os [and hence the outer core $^{186}Os/^{188}Os$ signature (*1*)] heterogeneously distributed within the source as veins. Because tungsten has a lower preference for solid metal than does Os (*26*), W and Os could be decoupled by fractional crystallization of the Fe-FeS melts. Thus, coupling between $^{182}W/^{184}W$, $^{186}Os/^{188}Os$, and Fe/Mn is not a prerequisite for evidence of core-mantle interaction.

Seismic studies indicate a correlation between ultralow-velocity zones (ULVZs) at the CMB, interpreted to be regions of partial melt, and the distribution of hot spots at the surface (*27*). There also appear to be rigid zones at the top of the core that correspond with ULVZs in the CMB region (*28*) that may be sites of FeO release from the core (*5*). Thus, the sources of mantle plumes originating from the CMB may have been affected by FeO metasomatism. This is the most tenable explanation at present for the observed excess of Fe/Mn in the Hawaiian lavas. Notably, Iceland neither is associated with a ULVZ (*29*) nor exhibits high Fe/Mn.

Table 1 shows that the observed Fe/Mn ratio in the Hawaiian lavas corresponds to a lower Mg# (88) than average upper mantle (Mg# = 89). This Mg# is within the 1σ range of measured Mg#'s of upper mantle peridotites [89 ± 2 (*13*)]. The higher FeO content implies a higher density, +0.5% relative to MORB mantle. This density contrast is about twice that estimated from seismic tomography models (*12*) but is sensitive to the choice of MORB Fe/Mn for normalization (Table 1). It is important to observe that our estimate of the density anomaly $\delta\rho/\rho$ does not include the effect of Fe enrichment due to recycling crust with a Fe/Mn ~ 60 because this contribution is not resolved by our technique. However, core-mantle interaction appears to have added enough FeO to the Hawaiian plume source to account for some (*10*) or all (*11*, *12*) of the geophysically observed density excess in the lower mantle. Thus, Fe/Mn analysis of hot spot lavas provides geochemical "ground truth" to geodynamical models of mantle circulation based on seismic tomography (*12*, *29*).

References and Notes

1. A. D. Brandon, M. D. Norman, R. J. Walker, J. W. Morgan, *Earth Planet. Sci. Lett.* **174**, 25 (1999).
2. E. Knittle, R. Jeanloz, *Science* **251**, 1438 (1991).
3. D. Walker, *Geochim. Cosmochim. Acta* **64**, 2897 (2000).
4. D. C. Rubie, C. K. Gessmann, D. J. Frost, *Nature* **429**, 58 (2004).
5. I. S. Puchtel, M. Humayun, *Geochim. Cosmochim. Acta* **64**, 4227 (2000).
6. B. Buffett, E. J. Garnero, R. Jeanloz, *Science* **290**, 1338 (2000).
7. A. Schersten, T. Elliott, C. Hawkesworth, M. Norman, *Nature* **427**, 234 (2004).
8. G. Ravizza, J. Blusztajn, H. M. Prichard, *Earth Planet. Sci. Lett.* **188**, 369 (2001).
9. A. D. Brandon *et al.*, *Earth Planet. Sci. Lett.* **206**, 411 (2003).
10. L. H. Kellogg, B. H. Hager, R. D. van der Hilst, *Science* **283**, 1881 (1999).
11. E. J. Garnero, *Annu. Rev. Earth Planet. Sci.* **28**, 509 (2000).
12. A. M. Forte, J. X. Mitrovica, *Nature* **410**, 1049 (2001).
13. W. F. McDonough, S.-s. Sun, *Chem. Geol.* **120**, 223 (1995).
14. C. H. Langmuir, G. N. Hanson, *Philos. Trans. R. Soc. London Ser. A* **297**, 383 (1980).
15. A. Ruzicka, G. A. Snyder, L. A. Taylor, *Geochim. Cosmochim. Acta* **65**, 979 (2001).
16. Materials and methods are available as supporting material on *Science* Online.
17. M. D. Norman, M. O. Garcia, *Earth Planet. Sci. Lett.* **168**, 27 (1999).
18. M. J. Walter, *J. Petrol.* **39**, 29 (1998).
19. M. Pertermann, M. M. Hirschmann, *J. Geophys. Res.* **108**, 2125, 10.1029/2000JB000118 (2003).
20. M. Pertermann, M. M. Hirschmann, *J. Petrol.* **44**, 2173 (2003).
21. T. Kogiso, M. M. Hirschmann, D. J. Frost, *Earth Planet. Sci. Lett.* **216**, 603 (2003).
22. J.-P. Poirier, *Phys. Earth Planet. Inter.* **85**, 319 (1994).
23. Experimental results of Rubie *et al.* (*4*) were extrapolated to 128 to 136 GPa and 2600 to 3000K with the use of their equation 2 to obtain the molar metal-silicate partition coefficient, $K_d \leq 6 \times 10^{-4}$. Setting $X_{Fe}^{metal} \sim 1$, $X_{FeO}^{Mg\text{–}wüstite} \sim 0.2$, where X represents the mole fraction, in their definition of K_d yields $X_O^{metal} \leq 1 \times 10^{-4}$. These experiments imply that metallic liquids in equilibrium with lower mantle mineralogy should be very low in oxygen content and that FeO should be released from the core to the mantle at the CMB, if oxygen is present in the outer core at 9 weight percent (wt %) (FeO = 40 wt %) (*22*).
24. T. Lay, Q. Williams, E. J. Garnero, *Nature* **392**, 461 (1998).
25. A. M. Jellinek, M. Manga, *Nature* **418**, 760 (2002).
26. N. L. Chabot, A. J. Campbell, J. H. Jones, M. Humayun, C. B. Agee, *Meteoritics Planet. Sci.* **38**, 181 (2003).
27. Q. Williams, J. Revenaugh, E. Garnero, *Science* **281**, 546 (1998).
28. S. Rost, J. Revenaugh, *Science* **294**, 1911 (2001).
29. A. M. Jellinek, M. Manga, *Rev. Geophysics*. **42**, RG3002, 10.1029/2003RG000144 (2004).

30. We thank S. Sorenson (Smithsonian Institution) and A. T. Anderson for providing samples; A. J. Campbell for support on the Element; and A. D. Brandon, B. Buffett, M. Hirschmann, and C. Langmuir for comments and discussions. Constructive reviews by C.-T. Lee and P. Reiners are gratefully acknowledged. NSF EAR-0309786 (M.H.) supported this work.

Supporting Online Material

www.sciencemag.org/cgi/content/full/306/5693/91/DC1
Materials and Methods
Figs. S1 and S2
Tables S1 and S2
References

3 June 2004; accepted 17 August 2004

Toroidal Triblock Copolymer Assemblies

Darrin J. Pochan,[1]* Zhiyun Chen,[2]† Honggang Cui,[1]† Kelly Hales,[1]† Kai Qi,[2]† Karen L. Wooley[2]*

A stable phase of toroidal, or ringlike, supramolecular assemblies was formed by combining dilute solution characteristics critical for both bundling of like-charged biopolymers and block copolymer micelle formation. The key to toroid versus classic cylinder micelle formation is the interaction of the negatively charged hydrophilic block of an amphiphilic triblock copolymer with a positively charged divalent organic counterion. This produces a self-attraction of cylindrical micelles that leads to toroid formation, a mechanism akin to the toroidal bundling of semiflexible charged biopolymers such as DNA. The toroids can be kinetically trapped or chemically cross-linked. Insight into the mechanism of toroid formation can be gained by observation of intermediate structures kinetically trapped during film casting.

Simple self-assembly methods can produce a broad range of intricate bioinspired nanostructures from synthetic block copolymers in dilute solution. For example, robust vesicles have been constructed from amphiphilic diblock copolymers (*1*–*3*). By using block copolymers instead of low–molecular weight lipid amphiphiles, direct control over the membrane thickness is achieved and the ultimate toughness of the vesicle is consequently enhanced (*1*, *4*). Similarly, cylindrical micelles exhibit stiffness behavior that is directly dependent on the core chemistry (*5*) or chain length (*6*). Such cylindrical structures have been designed to display specific coronal chemistry for biomimetic inorganic phase nucleation (*7*, *8*). Many examples of spherical micellar assemblies also exist in which the particle size and function can be controlled by means of block copolymer segment designs (*9*). In addition to the classic geometries of sphere, cylinder, and bilayer membrane, dilute block copolymers

[1]Materials Science and Engineering and Delaware Biotechnology Institute, University of Delaware, Newark, DE 19716, USA. [2]Center for Materials Innovation and Department of Chemistry, Washington University in Saint Louis, One Brookings Drive, CB 1134, Saint Louis, MO 63130, USA.

*To whom correspondence should be addressed.
†These authors contributed equally to this work.

can create a diverse catalog of geometries, including helices (*10*), cylindrical networks (*11*, *12*), nanotubes (*13*, *14*), the hollow hoop (*15*), and the bowl-shaped micelle (*16*). This complexity is prominent when the assembly occurs in solvent mixtures (*13*, *15*–*17*).

Nature produces complex intermolecular structure with biomolecules, namely peptides and nucleic acids, through the control of biomolecular primary, secondary, tertiary, and quaternary structure. The presence of electrostatic charge in biomolecular primary structure provides natural systems with a molecular-level tool to control intramolecular conformation (secondary and tertiary structure) and intermolecular aggregation (quaternary structure) over nanoscopic and microscopic dimensions. Charged biopolymer organization, such as DNA (*18*) or f-actin (*19*), is being studied in order to understand in vivo processes, including DNA compaction and storage in the chromosome, or to develop bioinspired vehicles for gene therapy delivery, such as DNA/lipid complexes (*20*, *21*). A key factor in controlling the final charged biopolymer assembly structure is counterion valency. In DNA, multivalent counterions, including heavy metal salts or oligoamines, can produce hexagonally close-packed DNA at almost crystalline DNA densities (*22*). Importantly, when the DNA is in the presence of multivalent counterions and is sufficiently dilute (in order to prevent lateral intermolecular association), chains close-pack locally but produce toroidal bundles on the length scale of one-hundred to several hundred nanometers. This toroidal bundle formation is due to the semiflexible nature of DNA; the large persistence length (~50 nm) prevents the complete collapse of the self-attractive molecules into a compact globule. The situation is slightly different in f-actin, a much stiffer chain that has a persistence length in excess of several micrometers. Counterion multivalency also produces attraction between like-charged, stiff f-actin chains. However, these attractive interactions primarily produce close-packed bundles of extended chains (*23*). In some cases, f-actin rings can be formed in the presence of multivalent counterions, but the rings are very large (diameters of more than several micrometers) relative to those formed by DNA. This is believed to be the consequence of the much higher bending stiffness of f-actin due to its much larger persistence length (*24*).

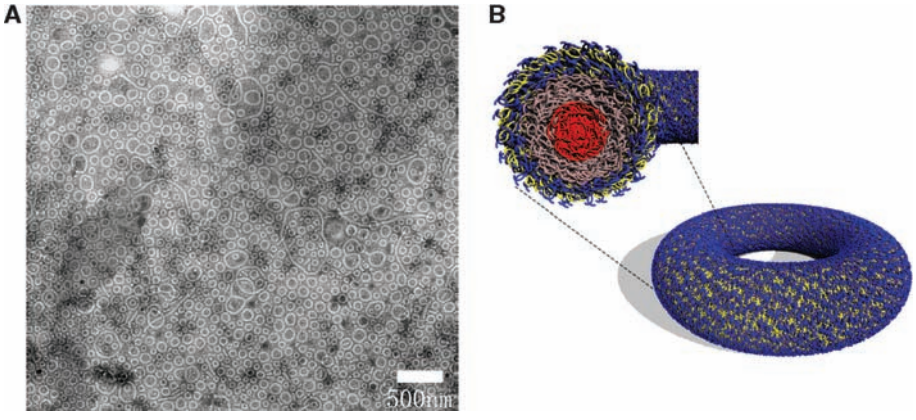

Fig. 1. (**A**) Low-magnification TEM image of toroidal micelle structure. This sample was cast from a solution with 0.1 wt % PAA_{99}-PMA_{73}-PS_{66} triblock copolymer, a THF:water volume ratio of 1:2, and an amine:acid molar ratio of 0.5:1 by addition of EDDA. The cast film was negatively stained with uranyl acetate. The toroidal micelles appear as light rings against a dark background. Although the micelle structure is overwhelmingly small rings (<200 nm in diameter), there exist a small minority of large rings, unclosed cylindrical micelles (appearing as white lines), and spherical micelles (appearing as light dots). (**B**) Cartoon schematic of toroidal micelle with cross section showing hydrophobic PS (red) and PMA (brown) core and hydrophilic PAA (yellow) corona with closely associated EDDA (blue).

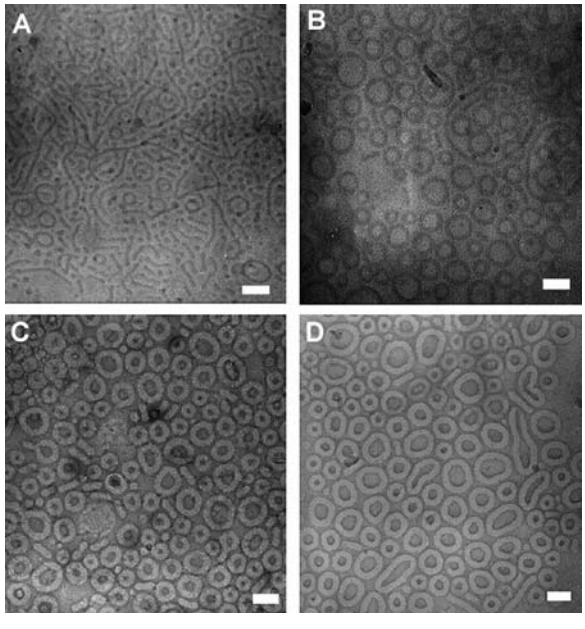

Fig. 2. TEM of PAA_{99}-PMA_{73}-PS_{66} micelles from 0.1 wt % triblock copolymer in solution of 1:2 by volume THF to water and 0.5:1 molar ratio of amine to acid. Scale bar, 100 nm. (**A**) CryoTEM of vitrified fresh solution showing mixture of cylindrical and spherical micelles with a small minority of toroids. The micelles appear dark against the vitrified solution background. (**B**) CryoTEM of the same solution as in (A) after allowing all of the THF to evaporate from the bulk solution showing predominantly a toroidal micelle structure. (**C**) Negatively stained TEM of a quickly cast film from solution in (A). Most of the micelles in (A) have transformed to toroidal micelles. (**D**) Negatively stained TEM of quickly cast film from solution in (B). The toroidal micelle structure is simply preserved on film casting.

We have combined synthetic block copolymer molecular design with solution conditions that favor self-attraction of charged semiflexible biopolymers to produce toroidal, or ring-shaped, micelles with a high degree of control and uniformity. The toroidal micelles are stable reproducible structures that are formed by the collapse of negatively charged cylindrical micelles, driven by interaction with a divalent organic cation. The assemblies are formed by a mixture of poly(acrylic acid–*b*–methyl acrylate–*b*-styrene) (PAA_{99}-PMA_{73}-PS_{66}) triblock copolymer amphiphile, water, tetrahydrofuran (THF), and 2,2′-(ethylenedioxy)diethylamine (EDDA). All four components are critical for toroid formation. Under optimized conditions, the toroidal phase is the predominant structure of the amphiphilic triblock copolymer, as seen from the low magnification transmission electron microscopy (TEM) micrograph of Fig. 1A, captured from a single layer of toroidal micelles drop cast from dilute suspension. Figure 1B illustrates the expected morphology that is generated in solutions composed predominantly of water; the hydrophobic PS and PMA are packaged within the core domain and are partially solvated by THF, and the hydrophilic PAA and hydrophilic but oppositely charged EDDA comprise the micelle corona.

A specific procedure was developed to produce the optimized conditions under which the toroids were formed and remained stable, ultimately in a mixture of water, THF, and EDDA. First, the triblock copolymer was allowed to dissolve in THF with a specific amount of EDDA that defined the molar ratio of amine:acid functionality between 0.5:1 and 1:1. Second, nanopure water was added dropwise to the solution with stirring

until the desired ratio of water to THF was reached. For eventual toroid formation, it was found that the water:THF volume ratio at this stage must be 1:1 < x < 4:1 and the polymer concentration should be dilute, with a value of <0.1 weight percent (wt %). The evaporation of THF from these solutions favored complete toroid formation and stability, but the THF was originally necessary for solvation of the core and transition between various assembly forms. The necessity for THF during supramolecular assembly transitions has been observed for vesicular fusion as well (*2*, *25*). Figure 2A contains cryoTEM data obtained from a solution with a volume ratio of water:THF = 2:1 and a molar ratio of amine:acid = 0.5:1. Under these conditions, a majority of cylinders were formed with only a minority of spherical and closed toroidal micelles. This low frequency of toroids has been observed in many cylindrical micelle systems (*11*, *26*, *27*). However, when the THF cosolvent was allowed to evaporate, a marked change in structure to predominantly toroids was observed. The THF was evaporated selectively by exposing the bulk solution to the laboratory atmosphere for several days, because THF has a considerably higher vapor pressure than that of water (129 mm Hg for pure THF versus 18 mm Hg for water at 20°C). CryoTEM data of the assemblies contained within the resulting aqueous suspension exhibited almost exclusively toroidal micelles (Fig. 2B). THF removal from the original suspension of Fig. 2A can be accelerated by casting a drop of micelle suspension directly onto a carbon-coated TEM sample grid. During drying over a period of 30 min, the THF again evaporated more rapidly than did the water. This allowed for reorganization of the assemblies into a thin film of overwhelmingly toroidal micelle structures (Fig. 2C). If a film of the suspension used for the cryogenic capture of the assemblies of Fig. 2B is cast directly onto a TEM grid and allowed to dry, then the toroid structure is preserved (Fig. 2D). Such stability suggests that the ring structure is kinetically trapped by the glassy state of the PS hydrophobic interior blocks of the toroids upon evaporation of the THF.

The mechanism of ring formation can be inferred by observing structures formed during the quick casting of films from water/THF suspensions (quickly going from the dominant cylindrical structure in Fig. 2A to the dominant toroidal structure in Fig. 2C). Although a majority of the structures formed by quick film casting are toroids, many intermediate structures (Fig. 3), rarely observed in cryoTEM experiments or in slowly evaporated solutions, are also formed. These structures include lariats, figure eights, dumbbells, and closed loops within the interior of cylindrical micelles, or combinations of these structures. In addition, cylinder ends that have come together but have not completely fused can be seen clearly because of the penetration of negative stain. These intermediates are dominated by trifunctional branch points as observed by Jain and Bates for nonionic diblock surfactants (*11*). However, unlike Jain and Bates, no network formation is observed, only toroidal micelles. The formation of intermediate structures and toroids appears to result from an identical mechanism, primarily the collapse of cylindrical micelles. This cylinder self-attraction is attributed to what can be considered the divalency of the oligodiamine EDDA [divalent cation at neutral pH in water resulting from primary amine p$K_a \approx 10$ (where K_a is the acid dissociation constant)] and the EDDA interaction with the carboxylates of the poly(acrylic acid) coronas (polyanionic at neutral pH in water with a p$K_a \approx 5$) of the cylindrical micelles. At amine:acid molar ratios of 0.5:1 to 1:1, the cylindrical micelles undergo a transition akin to the attractive toroidal bundling of DNA in the presence of multivalent counterions.

The cylinder collapse to rings cannot be exclusively end-to-end connection; this mechanism, predicted theoretically to form rings in cylindrical micelle suspensions with low critical micelle concentrations and high end-cap energies (*28*, *29*), has been only partially observed experimentally (*11–13*, *26*, *27*, *29*). End-to-end cylinder connection cannot be the exclusive ring-forming mechanism in the triblock system, primarily because the average toroid circumference is smaller than the contour length of the average cylindrical micelle (Fig. 2A). In addition, the existence of closed ring structures at the ends (Fig. 3, A, B, and G) and in the middle (Fig. 3, E, F, G, and I) of cylindrical micelles, along with lariat (Fig. 3, D, F, and H) and figure-eight structures (Fig. 3, C and J), is not possible through simple end-to-end connection of cylinders. Rather, these intermediates must be formed by the free end of a cylinder connecting to the midsection of a neighboring cylinder (or itself). Alternatively, severe cylinder buckling must occur to bring the body of the micelle in contact with itself in order to fuse together and form an internal ring structure. This is not to say that end-to-end connection of self-attractive cylinders does not take place. Indeed, the number of spherical micelles decreases as the solutions evaporate slowly (Figs. 1 and 2, B and D), suggesting that the spherical micelles are also attractive and fuse into cylinders that collapse into rings. In dilute polymer solution, the cylinder collapse is primarily from single cylindrical micelles leading to more regular ring structure. Quickly cast films result in an increased polymer concentration and more multicylinder collapse. The resulting multicylinder collapse may lead to single rings and the intermediate structures in Fig. 3.

The size and stability of the toroidal micelles can be influenced by the valency and concentration of organic counterion. For example, the valency of the organic counterion is critical in defining the ultimate structure formed. When PAA_{99}-*b*-PMA_{73}-*b*-PS_{66} suspensions were made with a 1:1 molar ratio of amine to acid with the use of a monoamine, 2-methoxyethylamine (essentially one-half of the EDDA unit), no closed ring structures were observed. Instead of a defined system of toroids with only a minority of remaining cylinders and spheres, small spherical micelles were formed (fig. S1A). Likewise, if the polymer was assembled in THF/water mixtures with little or no added divalent EDDA (<0.2:1 amine to acid), spherical micelles were also formed (fig. S1B). Therefore, the presence of an organic counterion and the valency of the counterion directly affect the geometry and the topology of micelles formed. In addition, the amine:acid functionality molar ratio can

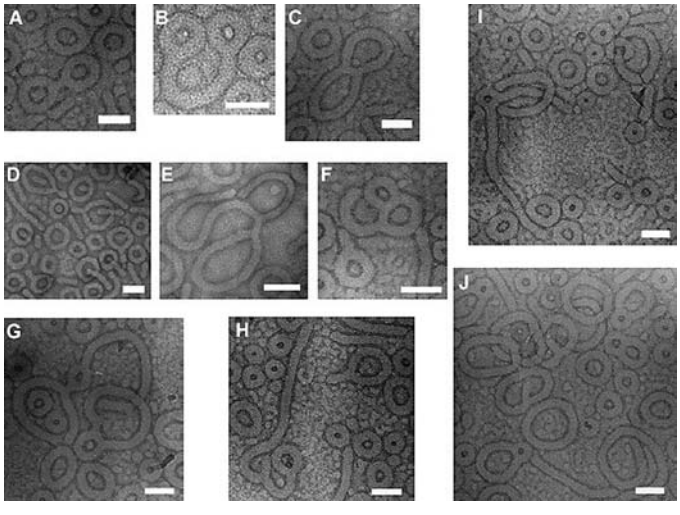

Fig. 3. (A to J) Negatively stained TEM data of intermediate structures formed by quick casting films from solutions containing 0.1 wt % PAA_{99}-PMA_{73}-PS_{66} triblock copolymer with a volume ratio of 1:2 THF to water and 0.5:1 molar ratio of amine to acid. Scale bar, 100 nm. Intermediate structures include dumbbells [(A), (B), and (G)], interior closed rings [(E), (F), (G), and (I)], lariats [(D), (F), and (H)], figure eights [(C) and (J)], and cylinders with ends connected but not fused together as indicated by the penetration of negative stain [(G) and (I)].

be altered to influence the ultimate size of the rings formed. As the relative ratio of amine to acid was increased from 0.5:1 to 1:1, the TEM images showed an increase in the average sizes of the ring micelles from a mean diameter for the overall structure of 98 to 126 nm, respectively (fig. S2). Images from either cryoTEM or negatively stained cast films revealed the same ring-size distribution, indicating that the toroids were formed in solution as a stable structure.

The toroidal micelles can be kinetically or chemically stabilized. During THF evaporation when self-attractive forces begin to dominate, sufficient THF swelling of the PS-PMA micelle cores exists to allow the formation of toroids through the fusion of cylindrical and spherical micelles. However, on complete THF evaporation (except for trace amounts contained in the micelle cores) the PS core resides below its glass transition, which, consequently, kinetically preserves the ring structure (compare Fig. 2, B and D). Alternatively, the toroids can be fixed chemically by means of cross-linking reactions on PAA coronal chains. In the presence of an activator, such as 1-[3′-(dimethylamino)propyl]-3-ethylcarbodiimide methiodide (DPEM), cross-linking occurs through the coupling of carboxylic acid moieties along the PAA backbone with N termini of the EDDA. Both chemical and physical toroid stabilization retain the average micelle size and distribution observed in solution (fig. S3).

Further evidence supporting like-charged attractive bundling as the mechanism for toroid formation can be found in the formation of another previously unrecognized structure observed in solutions with a low volume ratio of water to THF (<1:1 water to THF) and a 1:1 molar ratio of amine to acid. The cryoTEM in Fig. 4A reveals a suspension of flexible cylinders and spheres, presumably highly swollen with THF, exhibiting a low frequency of ring formation. However, upon slow casting of a film of this suspension, the cylinders and spheres collapse into close-packed bundles of cylinders (Fig. 4, B and C). Hexagonal symmetry can be observed in end-on projections of the cylinder bundles, whereas projections primarily perpendicular to the cylinder axes reveal the highly bent flexible nature of the cylindrical micelles during collapse (Fig. 4C) (*30*). During sample casting and THF evaporation, a critical solvent composition is attained in which attractive interactions between diamine and acid dominate, thus forming cylindrical micelles that collapse upon themselves. Importantly, the cylinders are flexible because they have hydrophobic cores that are swollen by THF. This flexibility allows the cylinders to collapse into dense bundles as shown in Fig. 4. This is in contrast with previously discussed toroid-forming solutions that begin with higher relative volume ratios of water to THF (>1:1 water to THF). These larger water:THF ratios produce PS and PMA cores that are relatively less swollen with THF, resulting in stiffer, semiflexible cylinders that cannot completely bundle on themselves during film casting. Rather, because of their higher bending stiffness, these micelles curl and fuse into toroidal micelles.

By combining parameters critical for (i) like-charged attraction bundling of biopolymers and (ii) block copolymer micelle formation in dilute solution, we produced a stable phase of toroidal micelles. The micelles are formed by a combination of cylindrical micelle curling and end-to-end collapse of cylindrical and spherical micelles. The size of the toroidal micelles can be influenced with the concentration of diamine counterion. The toroids can be kinetically trapped by ridding the system of organic solvent, thus taking the PS core block below its glass transition, or by chemically cross-linking the acid corona functionality.

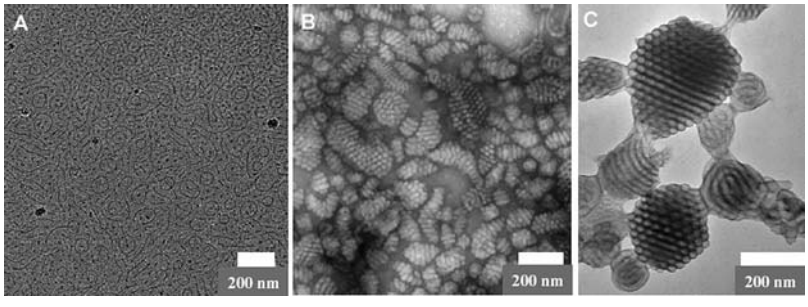

Fig. 4. TEM of PAA_{99}-PMA_{73}-PS_{66} micelles from 0.1 wt % triblock copolymer in 1:1 volume ratio of water to THF and 1:1 molar ratio amine to acid solution. (**A**) CryoTEM image of a cylindrical and spherical micelle mixture. (**B**) Negatively stained image of close-packed cylinder bundles formed during the casting of the solution from (A). (**C**) Higher magnification image of close-packed bundles. The electron imaging contrast between cylinders within the bundles is due to the penetration of the uranyl acetate negative stain between close-packed cylinders. The hexagonal symmetry from projections primarily parallel with the cylinder axes is clearly observed, as are projections more perpendicular to the cylinder axes appearing as a layered structure.

References and Notes

1. B. M. Discher *et al.*, *Science* **284**, 1143 (1999).
2. D. M. Vriezema *et al.*, *Angew. Chem. Int. Ed. Engl.* **42**, 772 (2003).
3. L. F. Zhang, A. Eisenberg, *Science* **268**, 1728 (1995).
4. H. Bermudez, A. K. Brannan, D. A. Hammer, F. S. Bates, D. E. Discher, *Macromolecules* **35**, 8203 (2002).
5. Y. Y. Won, H. T. Davis, F. S. Bates, *Science* **283**, 960 (1999).
6. P. Dalhaimer, H. Bermudez, D. E. Discher, *J. Polym. Sci. Part B Polym. Phys.* **42**, 168 (2004).
7. J. D. Hartgerink, E. Beniash, S. I. Stupp, *Science* **294**, 1684 (2001).
8. G. A. Silva *et al.*, *Science* **303**, 1352 (2004).
9. K. Prochazka, T. J. Martin, P. Munk, S. E. Webber, *Macromolecules* **29**, 6518 (1996).
10. J. Cornelissen, M. Fischer, N. Sommerdijk, R. J. M. Nolte, *Science* **280**, 1427 (1998).
11. S. Jain, F. S. Bates, *Science* **300**, 460 (2003).
12. S. Jain, F. S. Bates, *Macromolecules* **37**, 1511 (2004).
13. K. Yu, L. F. Zhang, A. Eisenberg, *Langmuir* **12**, 5980 (1996).
14. J. Raez, I. Manners, M. A. Winnik, *J. Am. Chem. Soc.* **124**, 10381 (2002).
15. L. F. Zhang, C. Bartels, Y. S. Yu, H. W. Shen, A. Eisenberg, *Phys. Rev. Lett.* **79**, 5034 (1997).
16. I. C. Riegel, A. Eisenberg, C. L. Petzhold, D. Samios, *Langmuir* **18**, 3358 (2002).
17. L. F. Zhang, A. Eisenberg, *J. Am. Chem. Soc.* **118**, 3168 (1996).
18. C. Bottcher, C. Endisch, J. H. Fuhrhop, C. Catterall, M. Eaton, *J. Am. Chem. Soc.* **120**, 12 (1998).
19. G. C. L. Wong *et al.*, *Science* **288**, 2035 (2000).
20. I. Koltover, T. Salditt, J. O. Radler, C. R. Safinya, *Science* **281**, 78 (1998).
21. K. Ewert *et al.*, *Curr. Med. Chem.* **11**, 133 (2004).
22. V. A. Bloomfield, *Biopolymers* **44**, 269 (1997).
23. J. X. Tang, P. A. Janmey, *J. Biol. Chem.* **271**, 8556 (1996).
24. J. X. Tang, J. A. Kas, J. V. Shah, P. A. Janmey, *Eur. Biophys. J Biophys. Lett.* **30**, 477 (2001).
25. D. M. Vriezema *et al.*, *Macromolecules* **37**, 4736 (2004).
26. A. Bernheim-Groswasser, R. Zana, Y. Talmon, *J. Phys. Chem. B* **104**, 4005 (2000).
27. J. T. Zhu, Y. G. Liao, W. Jiang, *Langmuir* **20**, 3809 (2004).
28. P. van der Schoot, J. P. Wittmer, *Macromol. Theor. Sim.* **8**, 428 (1999).
29. M. In, O. Aguerre-Chariol, R. Zana, *J. Phys. Chem. B* **103**, 7747 (1999).
30. The bundled cylinder particles are distinct from the hexagonal hollow hoop (HHH) structure observed by Zhang *et al.* (*15*). The interior structure of the HHH particles is actually similar to a bulk cylindrical phase in which cylinders of one block of a diblock polymer are locally hexagonally packed within a matrix of the other block. (However, the closed-hoop nature of the cylinder phase is unique to the HHH phase and is not observed in bulk cylindrical phases.) In contrast, the collapsed cylinders presented here are cylindrical micelles with a THF swollen PS/PMA core surrounded by a PAA corona complexed with diamine. The hexagonal packing does not arise from bulklike phase separation but from the intimate close-packing of the flexible cylindrical micelles.
31. We thank NSF for funding, specifically the Nanoscale Interdisciplinary Research Teams program under grant DMR-0210247. Any opinions, findings, conclusions, or recommendations expressed in this material are those of the authors and do not necessarily reflect the views of NSF. We thank J. L. Turner for creation of the toroid schematic in Fig. 1B. We also thank the W. M. Keck College of Engineering electron microscopy lab at the University of Delaware, nuclear magnetic resonance facilities of the Department of Chemistry and TEM facilities of Department of Physics at Washington University in Saint Louis.

Supporting Online Material

www.sciencemag.org/cgi/content/full/306/5693/94/DC1
Materials and Methods
Figs. S1 to S3
References

16 July 2004; accepted 7 September 2004